Vertical mode expansion method for numerical modeling of biperiodic structures

HUALIANG SHI[1,2], XUN LU[1], AND YA YAN LU[1,*]

[1] Department of Mathematics, City University of Hong Kong, Kowloon, Hong Kong
[2] Beijing Computational Science Research Center, No. 10 West Dongbeiwang Road, Haidian, Beijing, China
[*] Corresponding author: mayylu@cityu.edu.hk

Compiled March 29, 2016

Due to the existing nanofabrication techniques, many periodic photonic structures consist of different parts where the material properties depend only on one spatial variable. The vertical mode expansion method (VMEM) is a special computational method for analyzing the scattering of light by structures with this geometric feature. It provides two-dimensional (2D) formulations for the original three-dimensional problems. In this paper, two VMEM variants are presented for biperiodic structures with cylindrical objects of circular or general cross sections. Cylindrical wave expansions and boundary integral equations are used to handle the 2D Helmholtz equations that appear in the vertical mode expansion process. A number of techniques are introduced to overcome some difficulties associated with the periodicity. The method is relatively simple to implement, and highly competitive in terms of efficiency and accuracy.

OCIS codes: *(000.4430) Numerical approximation and analysis; (050.1755) Computational electromagnetic methods.*

http://dx.doi.org/

1. INTRODUCTION

Periodic structures such as diffraction gratings, photonic crystals and metamaterials, appear in numerous photonic devices. A number of mathematical problems are related to the modeling and analysis of periodic structures. An important problem is to analyze the diffraction of plane waves impinging upon a biperiodic structure sandwiched between two homogeneous media. Standard numerical methods such as the finite-difference time-domain (FDTD) method and the frequency-domain finite element method (FEM) [1–4] are widely used, but they often require too much computer resources. For plasmonic structures with metallic components, FDTD requires a very small grid size and a very small time step, and must incorporate proper dispersion models for metals. FEM requires a small mesh size near sharp edges and high-index-contrast interfaces, and gives rise to large, complex, non-Hermitian and indefinite linear systems that may be expensive to solve. Volume or surface integral equation methods [5–8] have also been used to analyze biperiodic structures. However, these methods are somewhat complicated to implement, especially when the periodic structure contains multiple material interfaces.

For biperiodic structures with some geometric features, it is possible to develop special numerical or semi-analytic methods that are more efficient than the general methods. For example, semi-analytic methods based on spherical wave expansions can be used to analyze biperiodic arrays of spheres [9–12]. If the biperiodic structure consists of layers that are invariant in the z direction perpendicular to the plane of periodicity (the xy plane), numerical modal methods can be used [13–21]. In each z-invariant layer, the electromagnetic field is expanded in two-dimensional (2D) eigenmodes with their mode profiles depending on x and y. A discretization in z is avoided, but the eigenmodes must be solved numerically. The Fourier modal method [13–20] and the finite element modal method [21] solve the 2D vectorial eigenmodes based on Fourier series expansions and a 2D FEM, respectively. Unfortunately, the numerical modal methods are not very efficient for three-dimensional (3D) biperiodic structures with metallic components, because the eigenmodes have large variations in the horizontal plane, and many modes are needed to match the tangential field components between the layers. These 2D modes are vectorial and expensive to calculate. To accurately represent such a mode, it is necessary to keep many terms in the Fourier series, or use a larger number discretization points.

The vertical mode expansion method (VMEM) [22–24] is a recently developed computational method for analyzing 3D structures with material properties depending only on one spatial variable z in different regions of the 3D physical space. The key idea is to expand the electromagnetic field in each region in the corresponding one-dimensional (1D) modes with z-dependent mode profiles. It turns out that the "expansion coefficients" are functions of x and y, and satisfy scalar 2D Helmholtz equations. In [23] and [24], we considered circular and arbitrary cylindrical structures, respectively, where the scalar 2D Helmholtz equations are treated by cylindrical wave expansions and boundary integral equations, respectively. Similar to the surface integral equation method, VMEM reduces the original 3D scattering problem to a 2D problem formulated on surfaces, but it is relatively simple.

So far, VMEM has only been implemented for non-periodic 3D structures involving one or more cylindrical structures [23–27]. In this paper, we present two VMEM variants for biperiodic structures involving circular and arbitrary cylindrical objects. As in [23] and [24], we use cylindrical wave expansions and boundary integral equations to process the 2D Helmholtz equations, but the periodicity brings in some difficulties which lead to numerical instabilities and loss of accuracy for naive implementations. We develop techniques to stabilize the cylindrical wave expansions and maintain the high order accuracy of the boundary integral equations. The new VMEM is validated and illustrated by numerical examples involving dielectric and metallic slabs with a periodic array of air holes, and periodic arrays of metallic nanoparticles on a substrate.

2. PROBLEM FORMULATION

We consider structures that are periodic in both x and y directions with the same period L, where $\{x, y, z\}$ is a Cartesian coordinate system, z is identified as the vertical coordinate, and xy plane is the horizontal plane. Two simple examples are shown in Fig. 1, where the left and right panels depict a slab with a

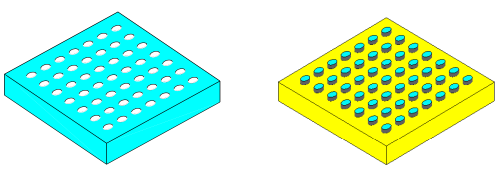

Fig. 1. Two biperiodic structures. Left: a slab with a periodic array of air holes. Right: a periodic array of particles on a substrate.

periodic array of air holes and a periodic array of particles on a substrate, respectively. We further assume that the main periodic part of the structure is bounded by two horizontal planes at $z = 0$ and $z = D$, and the top ($z > D$) and bottom ($z < 0$) media are homogeneous. Let ε and μ be the relative permittivity and relative permeability, respectively, we assume $\varepsilon = \varepsilon^{(t)}$, $\mu = \mu^{(t)}$ for $z > D$, and $\varepsilon = \varepsilon^{(b)}$, $\mu = \mu^{(b)}$ for $z < 0$, where $\varepsilon^{(t)}$, $\mu^{(t)}$, $\varepsilon^{(b)}$ and $\mu^{(b)}$ are real positive constants. The periodic structure has a unit cell which is assumed to be

$$S = \left\{ (x, y, z) \; : \; |x| < \frac{L}{2}, \; |y| < \frac{L}{2}, \; -\infty < z < \infty \right\}.$$

Notice that S is an infinitely-long cylinder and its cross section Ω is a square with side length L centered at the origin. For the second periodic structure shown in Fig. 1, the domain Ω is shown in Fig. 2.

The VMEM is applicable to structures for which the material properties are one-dimensional in different regions. In this paper, we assume S consists of two cylindrical regions S_0 and S_1 (with cross sections Ω_0 and Ω_1, respectively), such that

$$\varepsilon = \varepsilon^{(l)}(z), \; \mu = \mu^{(l)}(z), \quad (x, y, z) \in S_l, \tag{1}$$

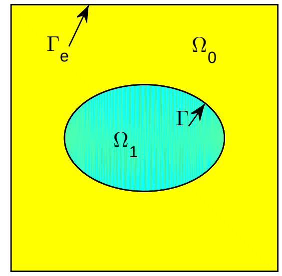

Fig. 2. Horizontal cross section Ω of a unit cell S for a biperiodic structure.

for $l = 0, 1$. For the first case shown in Fig. 1, S_1 and Ω_1 are related to the air hole, and S_0 and Ω_0 are related to the slab. The unit-cell cross section Ω contains exactly two subdomains Ω_0 and Ω_1. For simplicity, we assume Ω_0 encloses Ω_1. In that case, the boundary of Ω_1, denoted as Γ, is also the inner boundary of Ω_0. We denote the outer boundary of Ω_0 by Γ_e. Note that Γ_e is also the boundary of Ω and it consists of four edges as shown in Fig. 2. Of course, the definitions of $\varepsilon^{(l)}(z)$ and $\mu^{(l)}(z)$ must be consistent with the assumptions about the top and bottom media. Therefore, we must have $\varepsilon^{(l)}(z) = \varepsilon^{(t)}$, $\mu^{(l)}(z) = \mu^{(t)}$ for $z > D$, and $\varepsilon^{(l)}(z) = \varepsilon^{(b)}$, $\mu^{(l)}(z) = \mu^{(b)}$ for $z < 0$.

In the top homogeneous medium ($z > D$), we specify a plane incident wave $\{\mathbf{E}^{(i)}, \mathbf{H}^{(i)}\}$, where $\mathbf{E}$ is the electric field, $\mathbf{H}$ is a scaled magnetic field (the magnetic field multiplied by the free space impedance). The wave vector of the incident wave is $(\alpha_0, \beta_0, -\gamma_{00}^{(t)})$, where α_0 and β_0 are real,

$$\gamma_{00}^{(t)} = \sqrt{k_0^2 \varepsilon^{(t)} \mu^{(t)} - \alpha_0^2 - \beta_0^2}$$

is positive, and k_0 is the free space wavenumber. To analyze the diffraction of the incident wave, it is necessary to solve the linear frequency-domain Maxwell's equations:

$$\nabla \times \mathbf{E} = \mathrm{i} k_0 \mu \mathbf{H}, \quad \nabla \times \mathbf{H} = -\mathrm{i} k_0 \varepsilon \mathbf{E}, \tag{2}$$

where ω is the angular frequency, the time dependence is $e^{-\mathrm{i}\omega t}$, and i is the imaginary unit.

3. VERTICAL MODE EXPANSION METHOD

In [23] and [24], the VMEM was presented for non-periodic structures involving a single layered cylindrical object surrounded by a layered background. For biperiodic structures, the VMEM follows the same six steps as follows.

1. For 1D media with $\varepsilon = \varepsilon^{(l)}(z)$ and $\mu = \mu^{(l)}(z)$ ($l = 0, 1$) and the given incident wave $\{\mathbf{E}^{(i)}, \mathbf{H}^{(i)}\}$, solve the Maxwell's equations and denote the solutions as $\{\mathbf{E}^{(l)}, \mathbf{H}^{(l)}\}$ (the 1D solutions).

2. Truncate z by perfectly matched layers, discretize z by N points, solve the 1D vertical transverse electric (TE) and transverse magnetic (TM) modes $\phi_j^{(l,p)}(z)$, where $l \in \{0, 1\}$ is the location index, $p \in \{e, h\}$ is the polarization index, and $j \in \{1, 2, ..., N\}$ is the mode index. The corresponding propagation constants are $\eta_j^{(l,p)}$.

3. Discretize Γ by M points and approximate the tangential derivative operator along Γ by an $M \times M$ matrix $\mathbf{T}$ (the differentiation matrix).

4. For each triple (l, p, j) and function $V_j^{(l,p)}(x, y)$ satisfying the following 2D Helmholtz equation

$$\partial_x^2 V_j^{(l,p)} + \partial_y^2 V_j^{(l,p)} + [\eta_j^{(l,p)}]^2 V_j^{(l,p)} = 0 \quad \mathbf{(3)}$$

in Ω_l, find either the Dirichlet-to-Neumann (DtN) operator $\Lambda_j^{(l,p)}$ or the Neumann-to-Dirichlet (NtD) operator $\mathcal{N}_j^{(l,p)}$ (the inverse of $\Lambda_j^{(l,p)}$), satisfying

$$\Lambda_j^{(l,p)}\, V_j^{(l,p)}|_\Gamma = \partial_\nu V_j^{(l,p)}|_\Gamma, \quad \mathbf{(4)}$$

$$\mathcal{N}_j^{(l,p)}\, \partial_\nu V_j^{(l,p)}|_\Gamma = V_j^{(l,p)}|_\Gamma, \quad \mathbf{(5)}$$

where ∂_ν is the normal derivative operator on Γ. When Γ is discretized by M points, $\Lambda_j^{(l,p)}$ and $\mathcal{N}_j^{(l,p)}$ are approximated by $M \times M$ matrices.

5. Solve a linear system for all $V_j^{(l,p)}|_\Gamma$ or all $\partial_\nu V_j^{(l,p)}|_\Gamma$, depending on whether $\Lambda_j^{(l,p)}$ or $\mathcal{N}_j^{(l,p)}$ are available. The linear system involves $4NM$ unknowns.

6. Construct the solution $\{\mathbf{E}, \mathbf{H}\}$ based on the vertical mode expansions which involve the 1D solutions, the vertical modes, and the functions $V_j^{(l,p)}$, and calculate desired quantities such as transmittance and reflectance.

The key idea of the VMEM is to expand the field in regions S_0 and S_1 where ε and μ depend only on z. The 1D solutions of Step 1 are introduced, so that the differences between the total field and the 1D solutions exhibit outgoing behavior as $|z| \to \infty$, and satisfy homogeneous Maxwell's equations. The expansions involve the vertical modes $\phi_j^{(l,p)}(z)$ and the 2D unknown functions $V_j^{(l,p)}(x, y)$. The vertical modes are first calculated in Step 2, typically by a Chebyshev pseudospectral method [28]. Although the unknown functions $V_j^{(l,p)}$ are defined on 2D domains Ω_l, we only solve them (or their normal derivatives) on curve Γ in Step 5. The linear systems of Step 5 are established from the continuity conditions of tangential field components on the vertical boundary between S_0 and S_1. Since the tangential and normal derivatives of $V_j^{(l,p)}$ appear in the expansions, we approximate the tangential derivative operator ∂_τ by a matrix in Step 3, and calculate the DtN or NtD operators in Step 4. The matrix approximating the tangential derivative operator can be constructed by the Fourier pseudospectral method [28].

Steps 1-3 and 5 are identical to the non-periodic cases studied in [23] and [24]. The main difference appears in Step 4 in the construction of $\Lambda_j^{(l,p)}$ or $\mathcal{N}_j^{(l,p)}$ for domain Ω_0. In sections 4 and 5, we present the details of Step 4 for circular and arbitrary cylindrical objects, respectively. The periodicity also brings in some differences for Step 6, and they are described in section 6. We emphasize that although many DtN or NtD operators must be calculated in Step 4, they are associated with 2D Helmholtz equations, and the computing time for Step 4 is negligible compared with that for Step 5.

4. CIRCULAR CYLINDERS

In this section, we present a method to approximate the operators $\Lambda_j^{(l,p)}$ and $\mathcal{N}_j^{(l,p)}$ for periodic structures with circular cylindrical objects. Let a ($a < L/2$) be the radius of the cylinders, then Ω_1 is the circular disk given by $r = \sqrt{x^2 + y^2} < a$, and Ω_0 is the domain outside Ω_1 and inside the square Ω. In [23], we used cylindrical wave expansions to find the DtN operators for 2D Helmholtz equations in Ω_1 and in the infinite exterior domain Ω_∞ given by $r > a$. In the following, we show that cylindrical wave expansions can still be used to construct the DtN and NtD operators for domain Ω_0, but special care is needed to avoid numerical instability.

Due to the plane incident wave, the function $V_j^{(0,p)}$ satisfying Eq. (3) in Ω_0 (thus $l = 0$) must also satisfy the following quasi-periodic boundary conditions:

$$V_j^{(0,p)}(L/2, y) = e^{i\alpha_0 L} V_j^{(0,p)}(-L/2, y) \quad \mathbf{(6)}$$

$$\partial_x V_j^{(0,p)}(L/2, y) = e^{i\alpha_0 L} \partial_x V_j^{(0,p)}(-L/2, y) \quad \mathbf{(7)}$$

$$V_j^{(0,p)}(x, L/2) = e^{i\beta_0 L} V_j^{(0,p)}(x, -L/2) \quad \mathbf{(8)}$$

$$\partial_y V_j^{(0,p)}(x, L/2) = e^{i\beta_0 L} \partial_y V_j^{(0,p)}(x, -L/2), \quad \mathbf{(9)}$$

where α_0 and β_0 are the horizontal components of the incident wave vector. Our objective is to find the operators $\Lambda_j^{(0,p)}$ and $\mathcal{N}_j^{(0,p)}$ satisfying Eqs. (4) and (5) on Γ, where Γ is the circle $r = a$. To simplify the notations, we drop the subscript j and the superscript $(0, p)$ for $\eta_j^{(0,p)}$, $V_j^{(0,p)}$, $\Lambda_j^{(0,p)}$ and $\mathcal{N}_j^{(0,p)}$.

In Ω_0, a solution of Eq. (3) can be expanded in cylindrical waves as

$$V(x, y) = \sum_{m=-\infty}^{\infty} \left[a_m \frac{J_m(\eta r)}{J_m(\eta a)} + b_m \frac{Y_m(\eta r)}{Y_m(\eta a)} \right] e^{im\theta} \quad \mathbf{(10)}$$

where r and θ are the polar coordinates, J_m and Y_m are the mth order first and second kinds of Bessel functions, respectively. Expansions for $\partial_x V$, $\partial_y V$ and $\partial_r V$ can be easily obtained by taking the partial derivatives of Eq. (10). To find the DtN and NtD operators, we can follow the steps below.

1. Choose a positive integer $M_e = 4M_0$, discretize each edge of Γ_e by M_0 points, discretize Γ by $M = 4M_0$ points, and truncate the expansions for V, $\partial_x V$, $\partial_y V$ and $\partial_r V$ to M terms given by $-M/2 \le m \le M/2 - 1$.

2. Evaluate V and $\partial_r V$ at the M points on Γ by their truncated expansions, and obtain

$$\boldsymbol{v} = \mathbf{A}_{11}\boldsymbol{a} + \mathbf{A}_{12}\boldsymbol{b}, \quad \mathbf{(11)}$$

$$\partial_r \boldsymbol{v} = \mathbf{A}_{21}\boldsymbol{a} + \mathbf{A}_{22}\boldsymbol{b}, \quad \mathbf{(12)}$$

where $\boldsymbol{a}$ and $\boldsymbol{b}$ are column vectors of the retained expansion coefficients a_m and b_m, $\boldsymbol{v}$ and $\partial_r \boldsymbol{v}$ are column vectors of V and $\partial_r V$ at the M points on Γ, $\mathbf{A}_{11}$, $\mathbf{A}_{12}$, $\mathbf{A}_{21}$, and $\mathbf{A}_{22}$ are $M \times M$ matrices.

3. Evaluate Eqs. (6)-(9) at the $4M_0$ points on Γ_e by the truncated expansions of V, $\partial_x V$ and $\partial_y V$, and obtain

$$\mathbf{A}_{31}\boldsymbol{a} + \mathbf{A}_{32}\boldsymbol{b} = \mathbf{0}, \quad \mathbf{(13)}$$

where $\mathbf{A}_{31}$ and $\mathbf{A}_{32}$ are $M \times M$ matrices.

4. Solve $M \times M$ matrices $\mathbf{X}_{11}$, $\mathbf{X}_{12}$, $\mathbf{X}_{21}$ and $\mathbf{X}_{22}$ from the following equations

$$[\mathbf{X}_{11}, \mathbf{X}_{12}] \begin{bmatrix} \mathbf{A}_{11} & \mathbf{A}_{12} \\ \mathbf{A}_{31} & \mathbf{A}_{32} \end{bmatrix} = [\mathbf{A}_{21}, \mathbf{A}_{22}], \quad \textbf{(14)}$$

$$[\mathbf{X}_{21}, \mathbf{X}_{22}] \begin{bmatrix} \mathbf{A}_{21} & \mathbf{A}_{22} \\ \mathbf{A}_{31} & \mathbf{A}_{32} \end{bmatrix} = [\mathbf{A}_{11}, \mathbf{A}_{12}], \quad \textbf{(15)}$$

then the DtN and NtD operators are approximated by $\Lambda \approx \mathbf{X}_{11}$ and $\mathcal{N} \approx \mathbf{X}_{21}$, respectively.

In the second step above, we have $r = a$, since the points lie on Γ. The matrices $\mathbf{A}_{11}$ and $\mathbf{A}_{12}$ in Eq. (11) are identical, their entries are simply $e^{im\theta}$ for different m and θ. The expansion for $\partial_r V$ involves the derivatives of the Bessel functions. Since the derivative of a Bessel function of order m is related to Bessel functions of orders $m \pm 1$, we need to evaluate terms like $J_{m\pm1}(\eta a)/J_m(\eta a)$. As η is in general complex and its imaginary part (which should be nonnegative) can be quite large for some vertical modes, we use scaled Bessel functions defined as

$$\tilde{J}_m(z) = e^{-|\mathrm{Im}(z)|} J_m(z).$$

It then follows that

$$J_{m\pm1}(\eta a)/J_m(\eta a) = \tilde{J}_{m\pm1}(\eta a)/\tilde{J}_m(\eta a).$$

For the third step, each row in Eq. (13) corresponds to one of the conditions (6) - (9) for a pair of points on opposite edges of the boundary Γ_e, and these two points have the same value of r. Again, we use scaled Bessel functions which give rise to common factor $e^{\mathrm{Im}(\eta)(r-a)}$. This factor is removed in Eq. (13), so that the matrices $\mathbf{A}_{31}$ and $\mathbf{A}_{32}$ are better scaled.

Even with the above scalings, the $(2M) \times (2M)$ matrices in Eqs. (14) and (15) can be difficult to invert, because they are near singular when $\mathrm{Im}(\eta)$ is large. In that case, the solution of the Helmholtz equation (3) exhibit exponential behavior. If V or $\partial_r V$ is given on Γ, then V decays rapidly away from Γ, and it is almost zero on Γ_e. Therefore, the quasi-periodic conditions (6)-(9) are not so important when $\mathrm{Im}(\eta)$ is large. As a result, we may approximate the DtN or NtD operator for domain Ω_0 by the corresponding operator for the infinite domain Ω_∞ given by $r > a$. For Ω_∞, we expand the solution as

$$V(x,y) = \sum_{m=-\infty}^{\infty} c_m \frac{H_m^{(1)}(\eta r)}{H_m^{(1)}(\eta a)} e^{im\theta}, \quad r > a, \quad \textbf{(16)}$$

where $H_m^{(1)}$ is the mth order Hankel function of first kind. As described in [23], to find the DtN or NtD operator for Helmholtz equations in Ω_∞, we truncate Eq. (16) to M terms, evaluate V and $\partial_r V$ at the M points on Γ, and eliminate the coefficients c_m. In practice, we approximate the DtN and NtD operators for Ω_0 by those for Ω_∞ when $\mathrm{Im}(\eta)L > 60$.

5. ARBITRARY CYLINDERS

If the cylindrical regions S_1 and S_0 have more general cross sections (Ω_1 and Ω_0 as shown in Fig. 2), a fully numerical method is needed to calculate the DtN or NtD operators. In [24], we developed a boundary integral equation (BIE) method to compute the NtD operators for domains Ω_1 and Ω_∞ (the infinite domain outside Ω_1), assuming their boundaries are smooth. In this section, we extend the BIE method to domain Ω_0 which is bounded by Γ and Γ_e. The NtD operator $\mathcal{N}_j^{(0,p)}$ is defined on Γ for $V_j^{(0,p)}$ satisfying Eq. (3) in Ω_0 and the quasi-periodic conditions (6)-(9). As before, we assume Γ is smooth, but Γ_e has four corners. Therefore, the BIE method must be revised to incorporate the quasi-periodic conditions, and to take care of the corners so that the high accuracy of the method is maintained.

To simplify the notations, we drop the subscript and superscript for $V_j^{(0,p)}$, $\eta_j^{(0,p)}$, etc. For any $\boldsymbol{r} = (x,y)$ in Ω_0 and V satisfying Eq. (3), the Green's representation formula gives $V(\boldsymbol{r})$ in terms of V and $\partial_\nu V$ on the boundary of Ω_0, i.e., $\Gamma \cup \Gamma_e$, where $\partial_\nu V$ is the normal derivative of V. More precisely,

$$V(\boldsymbol{r}) = \int_{\Gamma\cup\Gamma_e} \left[G(\boldsymbol{r},\boldsymbol{r}') \frac{\partial V}{\partial \nu}(\boldsymbol{r}') - \frac{\partial G(\boldsymbol{r},\boldsymbol{r}')}{\partial \nu(\boldsymbol{r}')} V(\boldsymbol{r}') \right] ds(\boldsymbol{r}'), \quad \boldsymbol{r} \in \Omega_0, \quad \textbf{(17)}$$

where $\nu(\boldsymbol{r}')$ is the outward unit normal vector of $\Gamma \cup \Gamma_e$ at $\boldsymbol{r}'$, and G is the fundamental solution of the Helmholtz equation (3), i.e.,

$$G(\boldsymbol{r},\boldsymbol{r}') = \frac{\mathrm{i}}{4} H_0^{(1)}(\eta|\boldsymbol{r}-\boldsymbol{r}'|), \quad \boldsymbol{r} \neq \boldsymbol{r}'.$$

Taking the limit of Eq. (17) as $\boldsymbol{r}$ tends to points on $\Gamma \cup \Gamma_e$, one obtains the following BIE:

$$\frac{\rho(\boldsymbol{r})}{2} V(\boldsymbol{r}) = \int_{\Gamma\cup\Gamma_e} \left[G(\boldsymbol{r},\boldsymbol{r}') \frac{\partial V}{\partial \nu}(\boldsymbol{r}') - \frac{\partial G(\boldsymbol{r},\boldsymbol{r}')}{\partial \nu(\boldsymbol{r}')} V(\boldsymbol{r}') \right] ds(\boldsymbol{r}'), \quad \boldsymbol{r} \in \Gamma \cup \Gamma_e, \quad \textbf{(18)}$$

where $\rho(\boldsymbol{r})$ is the inner angle of the boundary at point $\boldsymbol{r}$ divided by π. If $\boldsymbol{r}$ is a smooth point on Γ or Γ_e, then $\rho(\boldsymbol{r}) = 1$. At the four corners of Γ_e, $\rho(\boldsymbol{r}) = 1/2$.

We assume the curves Γ and Γ_e are given periodically in parametric forms with period 1 as $\boldsymbol{r} = \boldsymbol{r}(t)$ for $0 \le t \le 1$ and $\boldsymbol{r} = \boldsymbol{r}_e(t)$ for $0 \le t \le 1$, respectively. For two positive integers M and M_e, we discretize these two curves by uniform samplings in t. More precisely, Γ is discretized as $\boldsymbol{r}_i = \boldsymbol{r}(i/M)$ for $0 \le i \le M$, and Γ_e is discretized as $\boldsymbol{r}_{e,i} = \boldsymbol{r}_e(i/M_e)$ for $0 \le i \le M_e$. To take care of the corners of Γ_e, we use a special formula for $\boldsymbol{r}_e(t)$, so that the discretization points have a much higher density near the corners. This so-called graded-mesh technique has been used in earlier works on 2D BIEs for domains with corners [29], and an explicit formula of $\boldsymbol{r}_e$ is given in Appendix A. With these discretizations, we have two vectors for V on Γ and Γ_e, respectively, namely,

$$\boldsymbol{v} = \begin{bmatrix} V(\boldsymbol{r}_1) \\ V(\boldsymbol{r}_2) \\ \vdots \\ V(\boldsymbol{r}_M) \end{bmatrix}, \quad \boldsymbol{v}_e = \begin{bmatrix} V(\boldsymbol{r}_{e,1}) \\ V(\boldsymbol{r}_{e,2}) \\ \vdots \\ V(\boldsymbol{r}_{e,M_e}) \end{bmatrix}. \quad \textbf{(19)}$$

We also have two vectors for $\partial_\nu V$ on Γ and Γ_e. For Γ_e, it is advantageous to scale $\partial_\nu V$ by $\sigma(t) = |\mathrm{d}\boldsymbol{r}_e(t)/\mathrm{d}t|$. Therefore, we have

$$\partial_\nu \boldsymbol{v} = \begin{bmatrix} \partial_\nu V(\boldsymbol{r}_1) \\ \partial_\nu V(\boldsymbol{r}_2) \\ \vdots \\ \partial_\nu V(\boldsymbol{r}_M) \end{bmatrix}, \quad \boldsymbol{w}_e = \begin{bmatrix} \sigma_1 \partial_\nu V(\boldsymbol{r}_{e,1}) \\ \sigma_2 \partial_\nu V(\boldsymbol{r}_{e,2}) \\ \vdots \\ \sigma_{M_e} \partial_\nu V(\boldsymbol{r}_{e,M_e}) \end{bmatrix}, \quad \textbf{(20)}$$

where $\sigma_j = \sigma(j/M_e)$.

Following the discretization process given in Appendix A, the BIE (18) is approximated by

$$\begin{bmatrix} \mathbf{A}_{11} & \mathbf{A}_{12} \\ \mathbf{A}_{21} & \mathbf{A}_{22} \end{bmatrix} \begin{bmatrix} v \\ v_e \end{bmatrix} = \begin{bmatrix} \mathbf{B}_{11} & \mathbf{B}_{12} \\ \mathbf{B}_{21} & \mathbf{B}_{22} \end{bmatrix} \begin{bmatrix} \partial_\nu v \\ w_e \end{bmatrix}, \tag{21}$$

where $\mathbf{A}_{11}$ is an $M \times M$ matrix, $\mathbf{A}_{12}$ is an $M \times M_e$ matrix, etc. The quasi-periodic conditions can be written as

$$\mathbf{C}_1 v_e = \mathbf{0}, \quad \mathbf{C}_2 w_e = \mathbf{0}, \tag{22}$$

where $\mathbf{C}_1$ and $\mathbf{C}_2$ are $(M_e/2) \times M_e$ matrices. To find the NtD map, we rewrite Eqs. (21) and (22) as

$$\begin{bmatrix} \mathbf{A}_{11} & \mathbf{A}_{12} & -\mathbf{B}_{12} \\ \mathbf{A}_{21} & \mathbf{A}_{22} & -\mathbf{B}_{22} \\ \mathbf{0} & \mathbf{C}_1 & \mathbf{0} \\ \mathbf{0} & \mathbf{0} & \mathbf{C}_2 \end{bmatrix} \begin{bmatrix} v \\ v_e \\ w_e \end{bmatrix} = \begin{bmatrix} \mathbf{B}_{11} \\ \mathbf{B}_{21} \\ \mathbf{0} \\ \mathbf{0} \end{bmatrix} \partial_\nu v, \tag{23}$$

and solve the linear system

$$\begin{bmatrix} \mathbf{A}_{11} & \mathbf{A}_{12} & -\mathbf{B}_{12} \\ \mathbf{A}_{21} & \mathbf{A}_{22} & -\mathbf{B}_{22} \\ \mathbf{0} & \mathbf{C}_1 & \mathbf{0} \\ \mathbf{0} & \mathbf{0} & \mathbf{C}_2 \end{bmatrix} \begin{bmatrix} \mathbf{X}_1 \\ \mathbf{X}_2 \\ \mathbf{X}_3 \end{bmatrix} = \begin{bmatrix} \mathbf{B}_{11} \\ \mathbf{B}_{21} \\ \mathbf{0} \\ \mathbf{0} \end{bmatrix},$$

where $\mathbf{X}_1$ is an $M \times M$ matrix that approximates the NtD operator $\mathcal{N}$.

In the above, $\nu(\boldsymbol{r})$ is an outward unit normal vector of Ω_0, it thus points into Ω_1 for $\boldsymbol{r} \in \Gamma$. To be consistent with section 4 and our previous work [24], we may reset $\nu(\boldsymbol{r})$ on Γ as the unit normal vector pointing into Ω_0. In that case, $\mathcal{N}$ should be approximated by $-\mathbf{X}_1$.

6. TRANSMISSION AND REFLECTION COEFFICIENTS

After the DtN or NtD operators are calculated, we set up and solve a linear system[1] for either $V_j^{(l,p)}$ on Γ [23] or $\partial_\nu V_j^{(l,p)}$ on Γ [24]. After that, $V_j^{(l,p)}$ in Ω_l can be evaluated using cylindrical wave expansions such as Eq. (10), or the Green's representation formula Eq. (17). The total field or the transmitted and reflected waves can be further evaluated using the vertical mode expansions [23, 24]. In [23], it is shown that the transmitted or reflected power can be evaluated by some integrals along Γ. That method remains valid for periodic problems where the field satisfies the quasi-periodic conditions (6)-(9). In the following, we present a simpler approach that first calculates the coefficients of the diffraction orders.

For an incident wave with the given wavevector $(\alpha_0, \beta_0, -\gamma_{00}^{(t)})$, the reflected and transmitted waves can be expanded in plane waves with wavevectors $(\alpha_m, \beta_n, \gamma_{mn}^{(t)})$ and $(\alpha_m, \beta_n, -\gamma_{mn}^{(b)})$, respectively, where

$$\alpha_m = \alpha_0 + \frac{2\pi m}{L}, \tag{24}$$

$$\beta_n = \beta_0 + \frac{2\pi n}{L}, \tag{25}$$

$$\gamma_{mn}^{(t)} = \sqrt{k_0^2 \varepsilon^{(t)} \mu^{(t)} - \alpha_m^2 - \beta_n^2}, \tag{26}$$

$$\gamma_{mn}^{(b)} = \sqrt{k_0^2 \varepsilon^{(b)} \mu^{(b)} - \alpha_m^2 - \beta_n^2}. \tag{27}$$

These are the (m, n)th reflected and transmitted diffraction orders, respectively, and they carry power only when they are propagating, that is, when $\gamma_{mn}^{(t)}$ or $\gamma_{mn}^{(b)}$ are real. The coefficients of these diffraction orders can be determined from the Fourier series of the reflected and transmitted waves at a fixed $z \geq D$ and $z \leq 0$, respectively. Since there are two linearly independent plane waves for a given wavevector, we need to determine the Fourier coefficients for two field components.

The H_z and E_z components are related to $V_j^{(l,e)}$ and $V_j^{(l,h)}$, respectively. To find their Fourier coefficients, we need to evaluate

$$\int_{\Omega_l} V_j^{(l,p)}(x, y) \Phi(x, y) \, \mathrm{d}\boldsymbol{r},$$

where $\Phi(x, y) = e^{-\mathrm{i}(\alpha_m x + \beta_n y)}$. Notice that

$$\partial_x^2 \Phi + \partial_y^2 \Phi + \kappa^2 \Phi = 0 \tag{28}$$

for $\kappa^2 = \alpha_m^2 + \beta_n^2$. Green's formula gives rise to

$$\left(\kappa^2 - [\eta_j^{(l,p)}]^2\right) \int_{\Omega_l} V_j^{(l,p)} \Phi \, \mathrm{d}\boldsymbol{r} = \int_{\partial\Omega_l} \left[\Phi \partial_\nu V_j^{(l,p)} - V_j^{(l,p)} \partial_\nu \Phi\right] \mathrm{d}s, \tag{29}$$

where $\partial\Omega_l$ is the boundary of Ω_l, and ∂_ν is the outward normal derivative operator. Notice that $\partial\Omega_1 = \Gamma$ and $\partial\Omega_0 = \Gamma \cup \Gamma_e$. While $V_j^{(0,p)}$ satisfies the quasi-periodic conditions (6)-(9), Φ satisfies the "reverse" quasi-periodic conditions, i.e., the complex conjugate of (6)-(9). As a result, it can be shown that the line integral on Γ_e is zero. Therefore, for both l, the line integral in Eq. (29) only needs to be evaluated on Γ.

For a normal incident wave, the z components of the $(0, 0)$th reflected and transmitted orders are zero. Therefore, we need to evaluate the Fourier coefficients for the x and y components of the wave field. In the vertical mode expansions [23], the horizontal field components are related to the partial derivatives of $V_j^{(l,p)}$ with respect to x and y. Therefore, we need to evaluate the integrals

$$\int_{\Omega_l} \partial_x V_j^{(l,p)} \Phi \, \mathrm{d}\boldsymbol{r}, \quad \int_{\Omega_l} \partial_y V_j^{(l,p)} \Phi \, \mathrm{d}\boldsymbol{r}.$$

Notice that

$$\int_{\Omega_l} \partial_x V_j^{(l,p)} \Phi \, \mathrm{d}\boldsymbol{r} = \int_{\partial\Omega_l} \nu_x V_j^{(l,p)} \Phi \, \mathrm{d}s - \int_{\Omega_l} V_j^{(l,p)} \partial_x \Phi \, \mathrm{d}\boldsymbol{r}, \tag{30}$$

where ν_x is the x component of the outward unit normal vector ν on $\partial\Omega_l$. The second term in the right hand side of Eq. (30) can be evaluated by a formula like (29), since $\partial_x \Phi$ satisfies the same Eq. (28). As before, for $l = 0$, the part of the line integral on Γ_e in Eq. (30) is zero. Therefore, the line integral only needs to be evaluated on Γ.

[1] There are some typos in the linear system for $V_j^{(l,p)}$ given on page 297 of [23]. In the equation for $A_{ij}^{(41)}$, $\phi_j^{(s,1)}$ should be $\phi_j^{(0,e)}$. In the equation for $A_{ij}^{(43)}$, $\phi_j^{(h,1)}$ should be $\phi_j^{(1,e)}$.

7. NUMERICAL EXAMPLES

In this section, we present a few numerical examples to validate and illustrate our method. The first example is a photonic crystal slab first analyzed by Fan and Joannopoulos [30]. It is a dielectric slab with a square lattice of circular air holes. The thickness of the slab and the radius of the holes are $D = 0.5L$ and $a = 0.2L$, respectively, where L is the lattice constant. The dielectric constant of the slab is $\varepsilon = 12$. Assuming the slab is surrounded by air and parallel to the xy plane, and the air holes are periodic in x and y directions, we calculate the transmission spectrum for a normal incident wave with its electric field in the x direction. Using the VMEM developed in previous sections, we obtain the spectrum shown in Fig. 3 where the horizontal

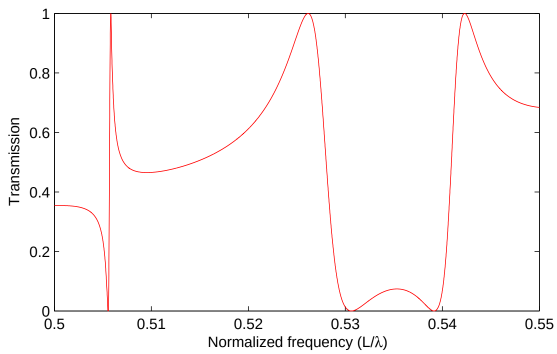

Fig. 3. Transmission spectrum of a photonic crystal slab with a square lattice of air holes.

axis is the normalized frequency $k_0L/(2\pi) = L/\lambda$, λ is the free space wavelength, and the vertical axis is the transmittance (the ratio between the transmitted power under a unit cell and the power of the incident wave impinging on the unit cell). Within the frequency range shown in Fig. 3, there are three total transmission peaks at normalized frequencies $L/\lambda = 0.5058, 0.5260$ and 0.5422. This problem has also been studied by Liu and Fan [20] and Dossou *et al.* [21], by a Fourier modal method and a finite element modal method, respectively. Our results are indistinguishable from those reported in [20] and [21]. In particular, the three peak frequencies are accurate to four significant digits.

For this example, the numerical results are obtained by the two versions of our method corresponding to sections 4 and 5, respectively. For the method based on cylindrical wave expansions, we discretize the z variable by $N = 75$ points and the circle Γ by $M = 28$ points. For the version based on the BIE, we use $N = 115$ points to discretize z, $M = 32$ points to discretize Γ, and $M_e = 120$ points to discretize Γ_e. Due to the reflection symmetries of the structure and the incident wave with respect to the x and y axes, the size of the final linear system can be reduced by a factor of 4.

The second example is a gold film with a periodic array of elliptic apertures on a glass substrate. The structure was first studied by Elliott *et al.* [31] for polarization control. The thickness of the gold film is 40 nm, and its refractive index is taken from [32]. The refractive index of the glass substrate is assumed to be 1.5163. The holes in the film form a square array which is periodic in the x and y directions with a period $L = 500$ nm. The main axes of the elliptic apertures are tilted to form 45° angles with the x and y axes, and their lengths are 500 nm and 250 nm, respectively. The top view of the structure and a unit cell are shown in Fig. 4. For this problem, we consider normal incident

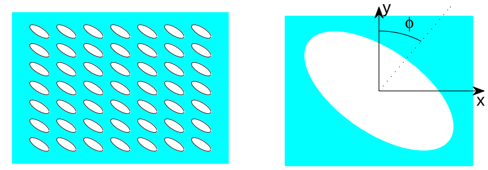

Fig. 4. A gold film with a periodic array of elliptic apertures on a glass substrate. Left: top view of the structure. Right: cross section of a unit cell.

plane waves given in the top medium (air). Let ϕ be the horizontal angle between the incident electric field and the y axis as shown in the right panel of Fig. 4, we show the transmission spectra for a number of incident waves with different ϕ in Fig. 5. Notice that the transmittance is independent of the horizontal angle for two wavelengths around 720 nm and 800 nm. These results are obtained by the BIE version of the VMEM using $N = 114$, $M = 32$ and $M_e = 128$, and they agree well with those reported in [31].

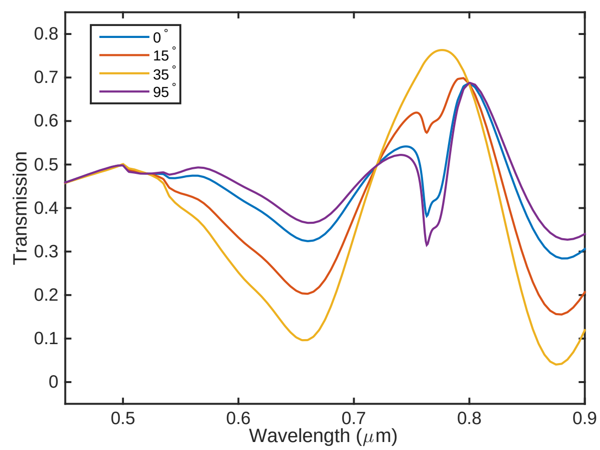

Fig. 5. Transmission spectra of a gold film with a periodic array of elliptic holes for incident waves with different horizontal angle ϕ.

The third example is a square periodic array of circular gold disks on a glass substrate and surrounded by water. The radius and height of the gold disks are $a = 90$ nm and $D = 40$ nm, respectively. The structure was previously studied by Chu *et al.* [33]. The refractive index of gold is taken from [34], and the refractive indices of glass and water are assumed to be 1.517 and 1.327, respectively. We consider a plane incident wave illuminating the device from the glass substrate at normal incidence, assuming the incident electric field is parallel to the x axis (one of the periodic directions). In Fig. 6, we show the extinction cross section for different values of the period L. Here, the extinction cross section is defined as $L^2(1 - T)$, where T is the transmittance. From Fig. 6, we can see that the period L is strongly related to the peak value and peak position of the extinction cross section. As the separation of the particles is increased, spectrum has a narrowing and red-shifting peak. Our results agree very well with the experimental results of [33]. For this example, we use the cylindrical wave expansion version of

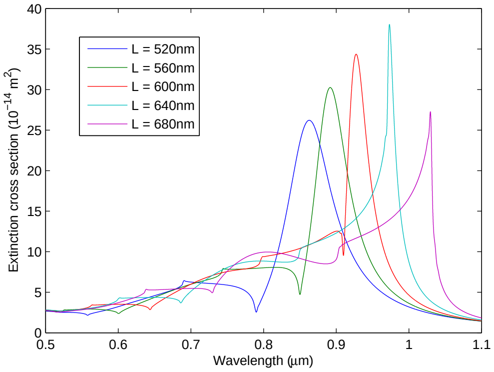

Fig. 6. Extinction spectra of a periodic array of gold disks for different period L.

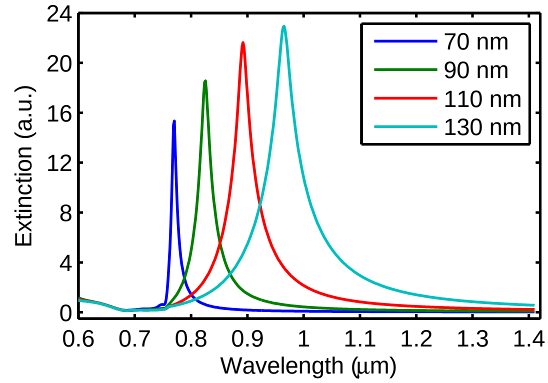

Fig. 8. Extinction spectra of a periodic array of gold elliptic cylinders for different semi-major axis R.

the VMEM, and discretize z by $N = 179$ points, and discretize the circle Γ by 32 points.

Finally, we follow Li *et al.* [35] and consider a periodic array of gold elliptic nanoparticles on a glass substrate. The nanoparticles have a height $D = 100$ nm, a 70 nm semi-minor axis, and a semi-major axis R. The refractive index of gold is taken from [32]. The structure is periodic in both x and y directions with period $L = 500$ nm, and is surrounded by a dielectric medium with refractive index 1.33. The refractive index of the glass substrate is assumed to be 1.5163. The top view of the structure and a unit cell are shown in Fig. 7. For a normal

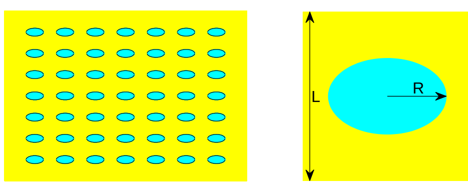

Fig. 7. A periodic array of gold elliptic cylinders on a glass substrate. Left: top view of the structure. Right: cross section of a unit cell.

incident plane wave given in the top medium with its electric field parallel to the x axis, we consider the effect of R on the extinction spectrum. Here, the extinction coefficient is defined as $-10 \times \log_{10}(T)$ where T is the transmittance. Using the BIE version of our method, we obtain the results shown in Fig. 8. As R is increased, the peak of the extinction spectrum exhibits a red-shift. Our results agree with those reported in [35], and they are obtained with $N = 156$, $M = 32$, and $M_e = 128$.

8. CONCLUSION

The VMEM is a special computational method to analyze 3D structures that are layered (i.e., material properties depend only on one spatial variable z) in different regions. In the previous sections, two VMEM variants are presented and validated for biperiodic structures sandwiched between two homogeneous media. These two variants are closely related to our early works on non-periodic structures [23, 24], and they rely on cylindrical wave expansions and BIEs (for 2D Helmholtz equations that appear in the expansion process), respectively. The periodicity gives rise to possible numerical instabilities for 2D Helmholtz equations with complex wavenumbers, and may reduce the order of accuracy of the BIEs due to the corners of the unit cells. In sections 4 and 5, we presented techniques to overcome these difficulties. The VMEM based on cylindrical wave expansions is only useful for structures with circular cylindrical objects, but it is simpler than the more general VMEM based on BIEs.

To simplify the presentation, we considered only structures that are periodic in x and y with the same period. This restriction can be easily removed. In particular, the method can be used to study structures with a triangular lattice of cylindrical objects. The method is also applicable to structures with more complicated unit cells, such as those with more than one cylindrical objects in each unit cell. Like the surface integral equation methods, the VMEM gives 2D formulations for 3D problems. Although it is necessary to calculate many DtN or NtD operators in Step 4 of the method, the most expensive step is to solve the final linear system (as in Step 5). For applications in nanoplasmonics, the size of the linear system is often not very large and can be further reduced by symmetry considerations. To further extend the capability of the VMEM, it is worthwhile to develop a fast iterative method for the linear system

APPENDIX A

The boundary Γ_e of the square Ω is first parameterized by its arclength s as follows:

$$\boldsymbol{r} = (x, y) = \begin{cases} (-L/2 + s, -L/2), & 0 \le s \le L, \\ (L/2, -3L/2 + s), & L \le s \le 2L, \\ (5L/2 - s, L/2), & 2L \le s \le 3L, \\ (-L/2, 7L/2 - s), & 3L \le s \le 4L. \end{cases}$$

To obtain the parametric representation $\boldsymbol{r} = \boldsymbol{r}_e(t)$ used in the graded mesh technique, we let s be a function of t, such that $s(\tau_j) = s_j$ for $0 \le j \le 4$ where $s_j = jL$ and $\tau_j = j/4$, and require that the first a few derivatives of $s(t)$ vanish at τ_j [29]. An explicit formula for $s(t)$ is

$$s(t) = \frac{s_j w_1^p + s_{j-1} w_2^p}{w_1^p + w_2^p}, \quad \tau_{j-1} \le t \le \tau_j, \quad 1 \le j \le 4,$$

where $p \geq 2$ is a parameter, and

$$w_1 = \left(\frac{1}{2} - \frac{1}{p}\right)\xi^3 + \frac{\xi}{p} + \frac{1}{2}, \quad w_2 = 1 - w_1,$$
$$\xi = \frac{2t - \tau_{j-1} - \tau_j}{\tau_j - \tau_{j-1}}.$$

In Fig. 9, we show the function $s(t)$ for $p = 3$ and for t on

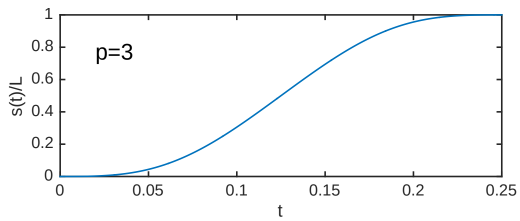

Fig. 9. Function $s(t)$ on $[0, 1/4]$ for $p = 3$.

$[\tau_0, \tau_1] = [0, 1/4]$. A simple translation gives $s(t)$ on other intervals.

Consider a boundary integral operator defined on $\Gamma \cup \Gamma_e$ by

$$f(\boldsymbol{r}) = \int_{\Gamma\cup\Gamma_e} K(\boldsymbol{r}, \boldsymbol{r}')g(\boldsymbol{r}')\, ds(\boldsymbol{r}'), \quad \boldsymbol{r} \in \Gamma \cup \Gamma_e, \tag{31}$$

where $K(\boldsymbol{r}, \boldsymbol{r}')$ is the kernel. For $\boldsymbol{r}_i \in \Gamma$, we have

$$f(\boldsymbol{r}_i) = \int_0^1 K(\boldsymbol{r}_i, \boldsymbol{r}(t))g(\boldsymbol{r}(t)) \left|\frac{d\boldsymbol{r}(t)}{dt}\right| dt + \int_0^1 K(\boldsymbol{r}_i, \boldsymbol{r}_e(t))g(\boldsymbol{r}_e(t)) \left|\frac{d\boldsymbol{r}_e(t)}{dt}\right| dt. \tag{32}$$

For the first term above, we approximate $g(\boldsymbol{r}(t))$ by its trigonometric interpolation, that is,

$$g(\boldsymbol{r}(t)) \approx \sum_{j=1}^{M} g(\boldsymbol{r}_j)L_M(t - t_j),$$

where $t_j = j/M$, $\boldsymbol{r}_j = \boldsymbol{r}(t_j)$ and

$$L_M(t) = \frac{\sin(M\pi t)}{M\tan(\pi t)}.$$

This leads to the integral

$$K_{ij}^{(11)} = \int_0^1 K(\boldsymbol{r}_i, \boldsymbol{r}(t)) \left|\frac{d\boldsymbol{r}(t)}{dt}\right| L_M(t - t_j)\, dt. \tag{33}$$

For the second integral in (32), we can approximate $g(\boldsymbol{r}_e(t))$ or $g(\boldsymbol{r}_e(t))\sigma(t)$ where $\sigma(t) = |d\boldsymbol{r}_e(t)/dt|$, by its trigonometric interpolation. For the latter case, we have

$$g(\boldsymbol{r}_e(t))\sigma(t) \approx \sum_{j=1}^{M_e} h_j L_{M_e}(t - t_{e,j}),$$

where $t_{e,j} = j/M_e$, $\boldsymbol{r}_{e,j} = \boldsymbol{r}_e(t_{e,j})$, and $h_j = g(\boldsymbol{r}_{e,j})\sigma(t_{e,j})$. Therefore, we need to evaluate

$$K_{ij}^{(12)} = \int_0^1 K(\boldsymbol{r}_i, \boldsymbol{r}_e(t))L_{M_e}(t - t_{e,j})\, dt. \tag{34}$$

In summary, Eq. (32) is approximated by

$$f(\boldsymbol{r}_i) \approx \sum_{j=1}^{M} K_{ij}^{(11)} g(\boldsymbol{r}_j) + \sum_{j=1}^{M_e} K_{ij}^{(12)} h_j.$$

Since $\boldsymbol{r}_i$ is not on Γ_e, the integrand in (34) is smooth, and we can use the standard trapezoidal rule. On the other hand, since $\boldsymbol{r}_i \in \Gamma$, if the kernel K has a logarithmic singularity at $\boldsymbol{r} = \boldsymbol{r}'$, then we can evaluate (33) by Alpert's hybrid Gauss-trapezoidal rule [24, 36].

For $\boldsymbol{r}_{e,i} \in \Gamma_e$, we may approximate Eq. (31) by

$$f(\boldsymbol{r}_{e,i}) \approx \sum_{j=1}^{M} K_{ij}^{(21)} g(\boldsymbol{r}_j) + \sum_{j=1}^{M_e} K_{ij}^{(22)} h_j,$$

where $K_{ij}^{(21)}$ and $K_{ij}^{(22)}$ are similarly defined, and they can be evaluated by the standard trapezoidal rule and Alpert's hybrid Gauss-trapezoidal rule, respectively.

In the right hand side of Eq. (18), we have two boundary integral operators with $G(\boldsymbol{r}, \boldsymbol{r}')$ and $\partial_\nu G(\boldsymbol{r}, \boldsymbol{r}')$ as the kernels. Both kernels have a logarithmic singularity at $\boldsymbol{r} = \boldsymbol{r}'$, and we can discretize these two integral operators following the general procedure given above.

FUNDING

The Research Grants Council of Hong Kong Special Administrative Region, China (CityU 11301914).

REFERENCES

1. X. Wei, A. J. Wachters, and H. P. Urbach, "Finite-element model for three-dimensional optical scattering problems," J. Opt. Soc. Am. A **24**, 866–881 (2007).
2. G. Demésy, F. Zolla, A. Nicolet, and M. Commandré, "All-purpose finite element formulation for arbitrarily shaped crossed-gratings embedded in a multilayered stack," J. Opt. Soc. Am. A **27**, 878–889 (2010).
3. G. Bao, P. Li, and H. Wu, "An adaptive edge element method with perfectly matched absorbing layers for wave scattering by biperiodic structures," Math. Comput. **79**, 1–34, (2010).
4. K. B. Dossou and L. C. Botten, "A combined three-dimensional finite element and scattering matrix method for the analysis of plane wave diffraction by bi-periodic, multilayered structures," J. Comput. Phys. **213**, 6969–6989 (2012).
5. M. C. van Beurden "Fast convergence with spectral volume integral equation for crossed block-shaped gratings with improved material interface conditions," J. Opt. Soc. Am. A **28**(11), 2269–2278 (2011).
6. A. A. Shcherbakov and A. V. Tishchenko, "New fast and memory-sparing method for rigorous electromagnetic analysis of 2D periodic dielectric structures," J. Quant. Spectrosc. Radiat. Transfer **113**, 158–171 (2012).
7. F. J. García de Abajo, "Retarded field calculation of electron energy loss in inhomogeneous dielectrics," Phys. Rev. B **65**, 115418 (2002).
8. A. M. Kern and O. J. F. Martin, "Surface integral formulation for 3D simulations of plasmonic and high permittivity nanostructures," J. Opt. Soc. Am. A **26**, 732–740 (2009).
9. A. Modinos, "Scattering of electromagnetic waves by a plane of spheres – formalism," Physica A **141**, 575–588 (1987).
10. N. Stefanou, V. Yannopapas, and A. Modinos, "MULTEM 2: A new version of the program for transmission and band-structure calculations of photonic crystals," Computer Physics Communications **132**, 189–196 (2000).
11. A. Matsushima, Y. Momoka, M. Ohtsu, and Y. Okuno, "Efficient numerical approach to electromagnetic scattering from three-dimensional periodic array of dielectric spheres using sequential accumulation," Progress in Electromagnetics Research **69**, 305–322 (2007).
12. H. Xie and Y. Y. Lu, "Improved spherical wave least squares method for analyzing periodic arrays of spheres," J. Opt. Soc. Am. A **27**, 1404–1412 (2010).
13. L. Li, "New formulation of the Fourier modal method for crossed surface-relief gratings," J. Opt. Soc. Am. A **14**, 2758–2767 (1997).

14. G. Granet and J. P. Plumey, “Parametric formulation of the Fourier modal method for crossed surface-relief gratings,” J. Opt. A **4**, S145–S149 (2002).
15. T. Schuster, J. Ruoff, N. Kerwien, S. Rafler, and W. Osten, “Normal vector method for convergence improvement using the RCWA for crossed gratings,” J. Opt. Soc. Am. A **24**, 2880–2890 (2007).
16. P. Gotz, T. Schuster, K. Frenner, S. Rafler, and W. Osten, “Normal vector method for the RCWA with automated vector field generation,” Opt. Express **16**, 17295–17301 (2008).
17. R. Antos, “Fourier factorization with complex polarization bases in modeling optics of discontinuous bi-periodic structures,” Opt. Express **17**, 7269-7274 (2009).
18. T. Weiss, G. Granet, N. A. Gippius, S. G. Tikhodeev, and H. Giessen, “Matched coordinates and adaptive spatial resolution in the Fourier modal method,” Opt. Express **17**, 8051–8061 (2009).
19. S. Essig and K. Busch, “Generation of adaptive coordinates and their use in the Fourier modal method,” Opt. Express **18**, 23258–23274 (2010).
20. V. Liu and S. Fan, “S^4: A free electromagnetic solver for layered periodic structures,” Computer Physics Communications **183**, 2233–2244 (2012).
21. K. B. Dossou, L. C. Botten, A. A. Asatryan, B. C. P. Sturmberg, M. A. Byrne, C. G. Poulton, R. C. McPhedran, and C. M. de Sterke, “Modal formulation for diffraction by absorbing photonic crystal slabs,” J. Opt. Soc. Am. A **29**, 817–831 (2012).
22. S. Boscolo and M. Midrio, “Three-dimensional multiple-scattering technique for the analysis of photonic-crystal slabs,” J. Lightw. Technol. **22**, 2778–2786 (2004).
23. X. Lu, H. Shi, and Y. Y. Lu, “Vertical mode expansion method for transmission of light through a single circular hole in a slab,” J. Opt. Soc. Am. A **31**, 293–300 (2014).
24. H. Shi and Y. Y. Lu, “Efficient vertical mode expansion method for scattering by arbitrary layered cylindrical structures,” Opt. Express **23**, 14618–14629 (2015).
25. H. Shi and Y. Y. Lu, “Vertical mode expansion method for analyzing elliptic cylindrical objects in a layered background,” J. Opt. Soc. Am. A **32**, 630–636 (2015).
26. X. Lu and Y. Y. Lu, “Analyzing bull’s eye structures by a vertical mode expansion method with rotational symmetry,” J. Opt. Soc. Am. B **32**, 2294–2298 (2015).
27. X. Lu and Y. Y. Lu, “Efficient method for analyzing multiple circular cylindrical nanoparticles on a substrate,” J. Opt. to appear.
28. L. N. Trefethen, *Spectral Methods in MATLAB* (Society for Industrial and Applied Mathematics, 2000).
29. D. Colton and R. Kress, *Inverse Acoustic and Electromagnetic Scattering Theory*, 3rd ed. (Springer-Verlag, 2013).
30. S. Fan and J. D. Joannopoulos, “Analysis of guided resonances in photonic crystal slabs,” Phys. Rev. B **65**, 235112 (2002).
31. J. Elliott, I. I. Smolyaninov, N. I. Zheludev, and A. V. Zayats, “Polarization control of optical transmission of a periodic array of elliptical nanoholes in a metal film,” Opt. Lett. **29**, 1414–1416 (2004).
32. A. D. Rakić, A. B. Djurišić, J. M. Elazar, and M. L. Majewski. “Optical properties of metallic films for vertical-cavity optoelectronic devices,” Appl. Opt. **37**, 5271–5283 (1998).
33. Y. Chu, E. Schonbrun, T. Yang, and K. B. Crozier, “Experimental observation of narrow surface plasmon resonances in gold nanoparticle arrays,” Appl. Phys. Lett. **93**, 181108 (2008).
34. E. D. Palik, *Handbook of Optical Constants of Solids* (Academic, 1998).
35. J. Li, Q. Kan, C. Wang, and H. Chen, “Effect of shape, height, and interparticle spacing of Au nanoparticles on the sensing performance of Au nanoparticle array,” Chinese Optics Letters **9**, 090501 (2011).
36. B. K. Alpert, “Hybrid Gauss-trapezoidal quadrature rules,” SIAM J. Sci. Comput. **20**(5), 1551–1584 (1999).